Astron. Nachr. / AN **328**, No. 10, 1009 – 1012 (2007) / **DOI** 10.1002/asna.200710837

Meridional flow profile measurements with SOHO/MDI

U. Mitra-Kraev⋆ and **M. J. Thompson**

University of Sheffield, Department of Applied Mathematics, Hicks Building, Sheffield, S3 7RH, UK

Received 2007 Sep 9, accepted 2007 Oct 30
Published online 2007 Dec 15

Key words Sun: helioseismology – Sun: interior – Sun: oscillations – methods: data analysis

We present meridional flow measurements of the Sun using a novel helioseismic approach for analyzing SOHO/MDI data in order to push the current limits in radial depth. Analyzing three consecutive months of data during solar minimum, we find that the meridional flow is as expected poleward in the upper convection zone, turns equatorward at a depth of around 40 Mm ($\sim 0.95\,R_\odot$), and possibly changes direction again in the lower convection zone. This may indicate two meridional circulation cells in each hemisphere, one beneath the other.

1 Introduction

The first observations of the Sun's meridional flow were made independently by Duvall (1979), Howard (1979), and Beckers (1979), who found a poleward drift of ∼20 m/s at the solar surface. By mass conservation, this meridional flow has to change direction somewhere in the solar interior, which may happen in the lower regions of the convection zone.

The meridional circulation plays an important role in many solar models. In mean-field models of angular momentum transport, the meridional circulation is responsible for how differential rotation is established and maintained (Rüdiger 1989; Thompson et al. 2003; Miesch 2005). Anisotropic Reynolds stresses, arising from random turbulent fluctuations of the plasma motions, can induce a meridional circulation, which in turn drives the differential rotation. In numerical simulations, Brun & Toomre (2002) find that the differential rotation profile is established by turbulent convection, and that the Reynolds stresses play a crucial role in transporting meridional momentum toward the equator. The meridional circulation is also an important ingredient in some dynamo models (Charbonneau 2005). In flux-transport models of the solar dynamo (Babcock-Leighton models) the meridional flow is needed to transport the surface poloidal magnetic field to the bottom of the convection zone, where it is then converted into a toroidal field by rotational shear (Dikpati & Charbonneau 1999).

Using helioseismic techniques, the meridional flow is usually observed in the upper layers of the solar convection zone. Quite good spatial resolution is achieved in this regime, in particular with ring-diagram analysis (e.g., González Hernández et al. 1999). Deeper down in the convection zone the horizontal resolution is poorer and to probe there the viewing angle needs to be large. No return flow has conclusively been observed to date. Using time-distance helioseismology, Giles (1999) measured the radial profile of the meridional circulation down to the bottom of the convection zone and, with the added constraint that the meridional circulation has to be contained within the convection zone, inferred a return flow at around 0.8 solar radii. Applying Hankel analysis, Braun & Fan (1998) saw a tentative return flow at around 40 Mm depth (but also consistent with zero within the error margin), whereas Duvall & Kosovichev (2001) observed no return flow.

2 Data and analysis

We analyze velocity data from the Michelson-Doppler Imager (MDI, Scherrer et al. 1995) on board the Solar and Heliospheric Observatory (SOHO, Domingo et al. 1995). The observations were taken during three consecutive Carrington Rotations: CR 1922 (1997 April 24 – May 21), CR 1923 (1997 May 21 – June 17), and CR 1924 (1997 June 17 – July 13). During this time, the Sun was at the minimum of its activity cycle. We use tracked data along the Center Meridian[1], obtained for the SOI Dynamics Campaign using high-resolution, full-disk Dopplergrams. The cadence is 60 s.

2.1 Dispersion relation along the center meridian

As our aim is to measure the meridional flow, which is in North-South direction, we restrict ourselves to analyzing spatially 1D data in the same direction. The data are co-added along latitude, resulting in a 2D array with one time and one spatial coordinate (see Mitra-Kraev et al. 2006). The spatial coordinate θ (latitude) is equally spaced in angle

⋆ Corresponding author: e-mail: u.mitrakraev@sheffield.ac.uk

[1] http://soi.stanford.edu/sssc/progs/mdi/track.html

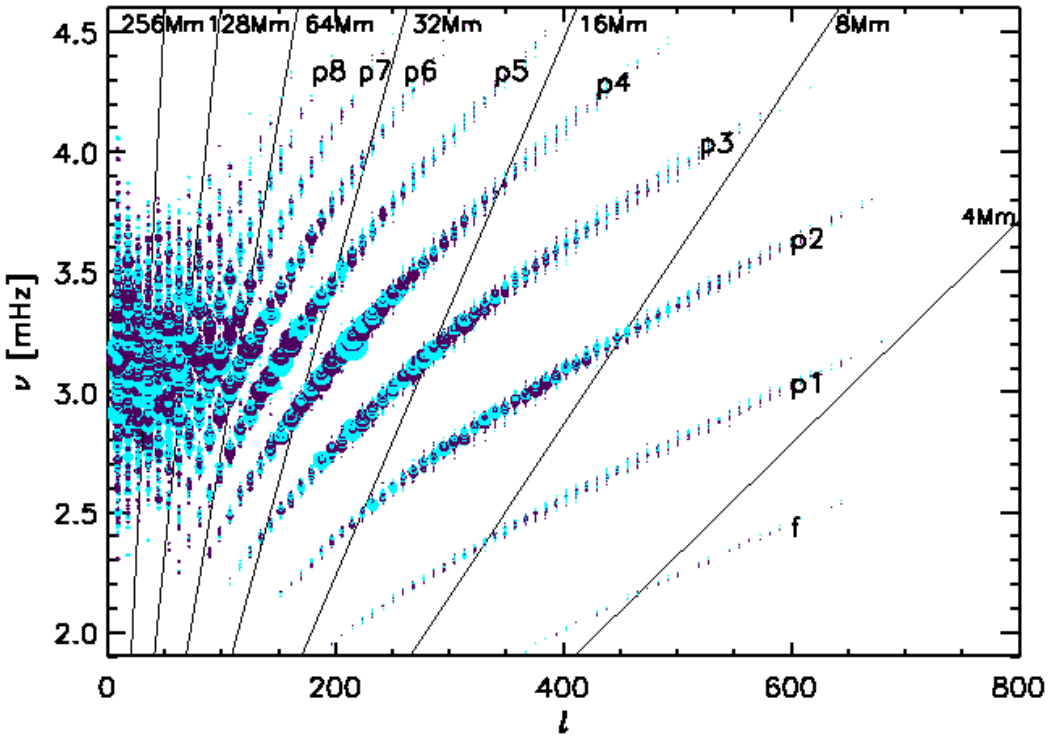

Fig. 1 The difference between the negative and the positive power spectrum, $P_{\rm neg} - P_{\rm pos}$. The frequency shift is visible along the f- and p-mode ridges. Dark dots are for $P_{\rm neg} > P_{\rm pos}$, while lighter dots are for $P_{\rm neg} < P_{\rm pos}$. Northward flow is present if the dark dots are shifted to higher frequencies and lighter dots to lower ones, while for Southward flow lighter dots are at higher frequencies than dark dots. The size of the dots is proportional to the absolute power. The black lines indicate the lower ray-turning points.

(spacing $\mathrm{d}\theta = 0.125°$). As the meridional flow is opposite in each hemisphere and vanishes around the equator, the range $+20°$ to $+60°$ is used for the Northern, and $-60°$ to $-20°$ for the Southern hemisphere. For each hemisphere we obtain a power spectrum

$$P(\nu, l) = \left|\widehat{f}(\nu, l)\right|^2,$$

where

$$\widehat{f}(\nu, k_\theta) = \sum f(t, \theta)\, \mathrm{e}^{-i(2\pi\nu t + k_\theta \theta)}$$

is the Fourier transform of the data $f(t, \theta)$. The power spectrum has symmetries such that $P(|\nu| > 0, |l| > 0) = P(|\nu| < 0, |l| < 0) \equiv P_{\rm pos}$, which we define as the 'positive', and $P(|\nu| > 0, |l| < 0) = P(|\nu| < 0, |l| > 0) \equiv P_{\rm neg}$, which we define as the 'negative' power spectrum. The difference between the positive and the negative power spectrum can be attributed to flows.

The approach of a 1D Fourier transform along the center meridian is comparable to a spherical harmonic treatment with only considering $m = 0$ modes, which was used by Krieger et al. (2007) for meridional flow measurements. As k_θ corresponds to the spherical harmonic degree l, we use the notation $k_\theta \equiv l$ from now on. With the observing length $T_{\rm obs} \approx 27\,\mathrm{days}$ and the latitudinal range $\theta_{\rm range} = 40°$, the resolutions are given by $\mathrm{d}\nu = 1/T_{\rm obs} \approx 0.4\,\mu\mathrm{Hz}$ and $\mathrm{d}l = 2\pi/\theta_{\rm range} \approx 9$.

2.2 The effect of flows on the p-mode ridges

For slow flows, which allow a linear approximation, the frequency splitting is given by $\Delta\omega = k_h \cdot U'$ (an expression which is also used in ring-diagram analysis) where k_h is the horizontal wave number and the velocity U' is the radially-dependent horizontal flow $U(r)$ convolved with a function describing the medium the pressure wave passes through. For measured $\Delta\omega$ as a function of k_h, $U(r)$ can be retrieved by an inversion.

In our case k_h, U' and $U(r)$ are 1D variables, describing the flow perpendicular to the solar radius in the North-South direction. With $\Delta\omega = 2\pi\Delta\nu$ and $k_h = l/R_\odot$ we obtain for the frequency shift in velocity units

$$U'(\nu/l) = \Delta\nu 2\pi R_\odot / l, \qquad (1)$$

where $R_\odot = 6.96 \times 10^8\,\mathrm{m}$ is the solar radius. The frequency shift $\Delta\nu$ is the shift by which, for a given l value, a p-mode ridge is displaced from its unperturbed position due to a flow. A Northward flow moves p-mode ridges along l, such that the frequency of p-mode ridges in the positive

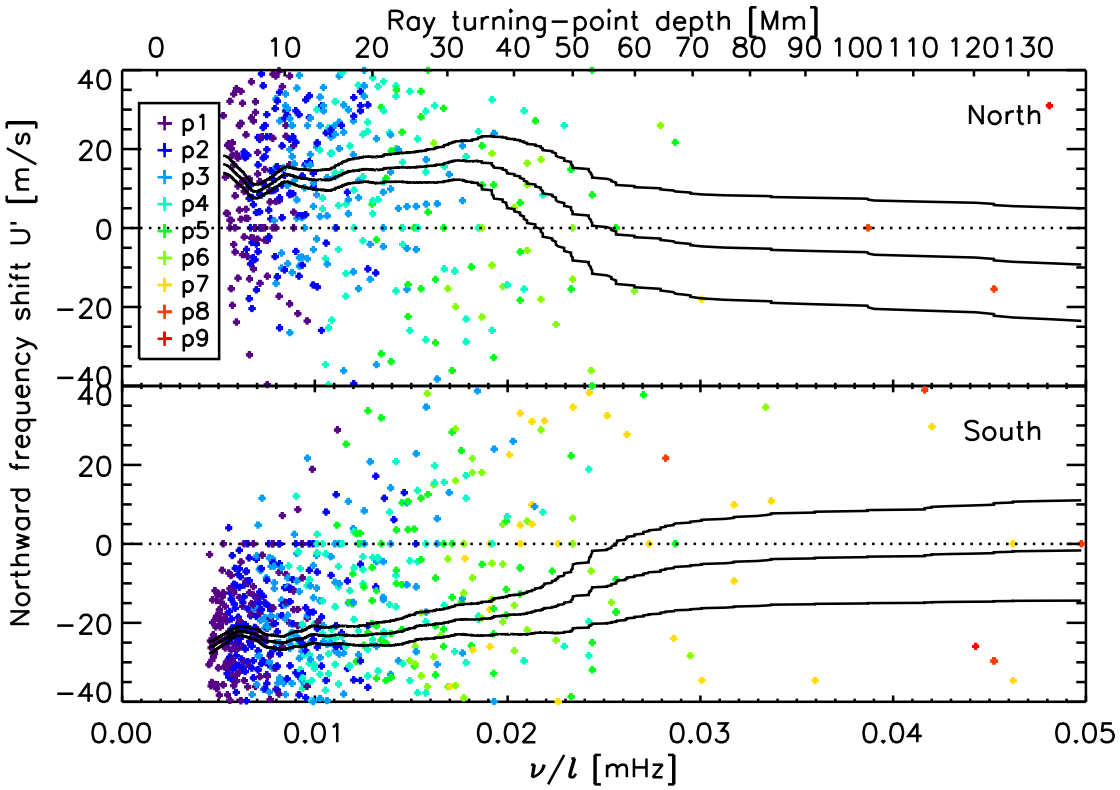

Fig. 2 The observed frequency shifts in the Northern (top) and Southern (bottom) hemispheres.

power spectrum is reduced by $\Delta\nu$, while the frequency of p-mode ridges in the negative power spectrum is enhanced by $\Delta\nu$.

Figure 1 shows the difference between the negative and the positive power spectrum, $P_{\rm neg} - P_{\rm pos}$, for the Southern hemisphere of CR 1922–1924. The size of the dots is linear with absolute spectral power. For better readability, all power smaller than a lower cutoff, which was chosen to decay exponentially along l and has a Lorentzian shape as a function of ν around 3.3 mHz, was set to zero. The f- and p-mode ridges are clearly visible due to the frequency shift. The f mode as well as p1–p8 modes are labeled. Dark dots are for $P_{\rm neg} - P_{\rm pos} > 0$, while lighter dots represent $P_{\rm neg} - P_{\rm pos} < 0$. This means a lighter dot being at a slightly larger frequency than its darker counterpart indicates a Southward flow, whereas a dark dot sitting at a larger frequency indicates a Northward flow. The straight black lines indicate the lower ray-turning points.

2.3 Measuring the frequency shift

In order to obtain the frequency shift $\Delta\nu$, we cross-correlate $P_{\rm neg}$ and $P_{\rm pos}$ for each l over a ν-range covering each p-mode ridge. The criterion for accepting a measurement is a correlation coefficient of 0.35 or more.

Figure 2 shows the measured frequency shift $U'(\nu/l)$ for the Northern (top panel) and Southern (bottom panel) hemispheres obtained for each power spectrum of the three Carrington rotations. The spread (-200 to $+400$ m/s) of the individual frequency shifts, represented by crosses and color coded with the corresponding p-mode, exceeds the plotting range. The middle black curve was obtained by smoothing the individual measurements twice with a bin size of 101 points. For the first smoothing, the error is given by the standard deviation of the points. The error margins in Figure 2 (upper and lower lines) are then given by error propagation in the second smoothing, assuming that the initial errors given by the standard deviation of the points are independent. However, as the initial errors are clearly not independent, this treatment undoubtedly underestimates the errors somewhat.

2.4 Asymptotic inversion

We invert the smoothed curve U' using an asymptotic inversion (see, e.g., Christensen-Dalsgaard et al. 1990). The inversion is given by

$$U(r) = \frac{-2a(r)}{\pi} \frac{\mathrm{d}}{\mathrm{d}\ln r} \int_{a(R_\odot)}^{a(r)} \sqrt{\frac{1}{a^2(r) - w^2}}\; U'(w)\, dw$$

with $w = 2\pi\nu/l$, r the solar radius, $a(r) = c(r)/r$, and $c(r)$ the sound-speed profile given by Model S of Christensen-Dalsgaard et al. (1996). The integral ranges from the solar surface to the lower turning point of the ray path. In order to solve the integral, which has an integrable singularity at the upper

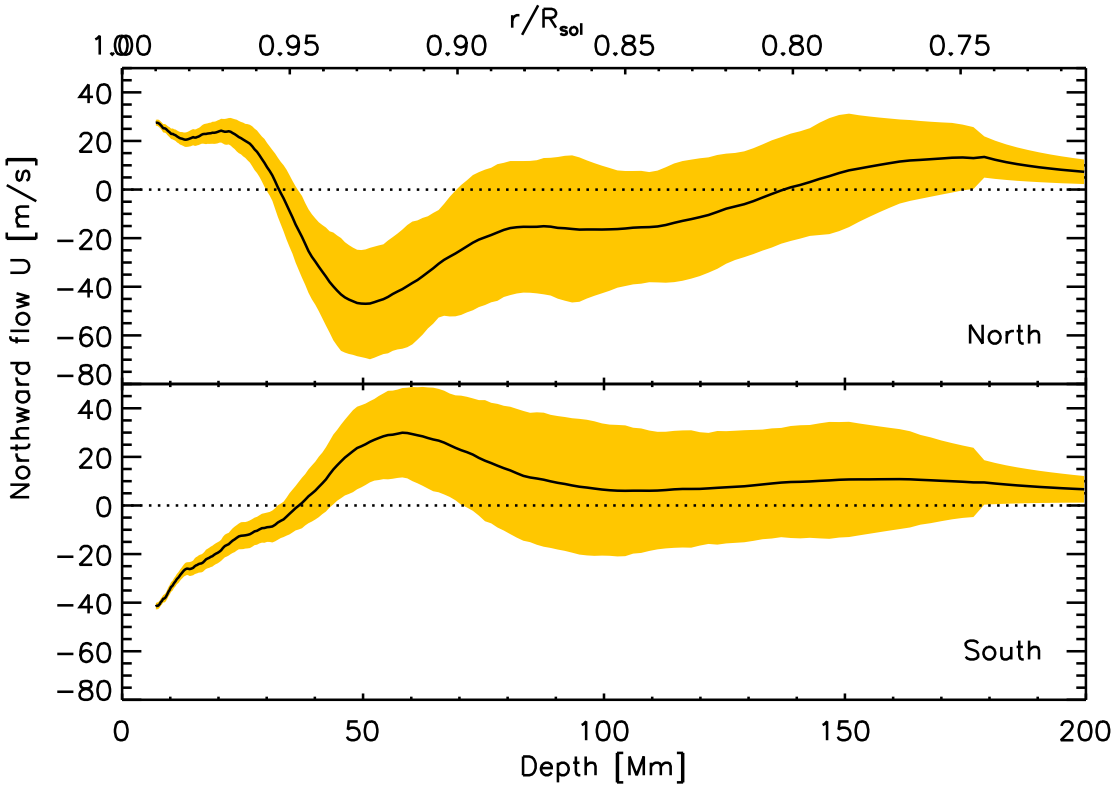

Fig. 3 The meridional flow profile for the Northern and Southern hemisphere obtained by asymptotic inversion.

boundary, the numerical scheme described in Appendix II of Christensen-Dalsgaard et al. (1989) was applied.

Figure 3 displays the obtained meridional flow profile from the asymptotic inversion. Displayed is the Northward flow for both the Northern and Southern hemispheres. The error region (shaded area) was obtained by Monte-Carlo simulations. The inversion profile was twice smoothed.

3 Discussion and conclusions

We analyzed high-resolution full-disk velocity data from SOHO/MDI along the center meridian covering three Carrington rotations from April to June 1997. Using a Fourier transform and measuring the frequency shift of the p-mode ridges in the power spectrum, we are able to obtain a meridional flow profile as a function of radius/depth. Figure 3 shows that in the Northern as well as the Southern hemisphere the flow is poleward close to the solar surface and turns equatorward at around 40 Mm. Such a return flow was previously tentatively observed by Braun & Fan (1998), analyzing data from the same period (but only for 8 days instead of 3 months). The flow may again turn poleward in deeper regions indicating a counter cell, although the data is also consistent with zero flow at lower regions. Such counter cells are consistent with recent numerical simulations (Miesch et al. 2007). The near-surface flow being somewhat larger in the Southern than in the Northern hemisphere may be because of the inclination of the solar rotation axis (Beck & Giles 2005).

Acknowledgements. We thank SOHO and in particular the SOI Team at Stanford University for making SOHO/MDI data readily available. We are also grateful to the UK Science and Technology Research Council (STFC) for funding this research.

References

Beck, J. G. & Giles, P. 2005, ApJ, 621, L153
Beckers, J. M. 1979, in Proc. Catania Workshop on Solar Rotation
Braun, D. C. & Fan, Y. 1998, ApJ, 508, 105
Brun, A. S. & Toomre, J. 2002, ApJ, 570, 865
Charbonneau, P. 2005, LRSP, 2, 2
Christensen-Dalsgaard et al. 1996, Science, 272, 1286
Christensen-Dalsgaard, J., Gough, D. O., & Thompson, M. J. 1989, MNRAS, 238, 481
Christensen-Dalsgaard, J., Schou, J., & Thompson, M. J. 1990, MNRAS, 242, 353
Dikpati, M. & Charbonneau, P. 1999, ApJ, 518, 508
Domingo, V., Fleck, B., & Poland, A. I. 1995, SoPh, 162, 1
Duvall, T. L. 1979, SoPh, 63, 3
Duvall, T. L. & Kosovichev, A. G. 2001, in IAUS No. 203, 159
Giles, P. M. 1999, PhD thesis, Stanford University
González Hernández, I. et al. 1999, ApJ, 510
Howard, R. 1979, ApJ, 228, L45
Krieger, L., Roth, M., & von der Lühe, O. 2007, AN, 328, 252
Miesch, M., Brun, A. S., DeRosa, M. L., & Toomre, J. 2007, ApJ, submitted, see also arXiv:0707.1460v1 [astro-ph]
Miesch, M. S. 2005, LRSP, 2, 1

Mitra-Kraev, U., Thompson, M. J., & Woodard, M. F. 2006, in ESASP No. 624, 57
Rüdiger, G. 1989, Differential Rotation and Stellar Convection (New York: Gordon and Breach), 328pp
Scherrer, P. H. et al. 1995, SoPh, 162, 129
Thompson, M. J., Christensen-Dalsgaard, J., Miesch, M. S., & Toomre, J. 2003, ARA&A, 41, 599